Climate Dynamics manuscript No.
(will be inserted by the editor)

The impact of an improved ice sheet freshwater flux representation on ocean heat storage

Marco A.J. Stoffelen

20 August 2015

Abstract Freshwater fluxes from the Greenland and Antarctic ice sheet might impact ocean circulation and thereby the distribution of heat in a warming climate. Despite their potential relevance, they are often not well represented in state-of-the-art climate models. Here, we incorporate a best estimate of freshwater runoff from both ice sheets into long-term (1850-2200) climate simulations by the Community Earth System Model (CESM), for both a strong (RCP8.5) and mild (RCP2.6) warming scenario. We analyze the differences with control simulations, focusing on the Atlantic meridional overturning circulation (AMOC), ocean heat uptake and global mean surface air temperature (GMST). Although the direct effects of the CO_2 forcing in the climate scenarios are dominant, the incorporation of realistic ice sheet freshwater fluxes has a significant impact on the heat uptake and distribution in the ocean. Antarctic Bottom Water formation is significantly affected, causing a vertical redistribution of heat during the historical period that leads to warmer deep waters and negative GMST anomalies that are on the order of 0.2 K. In the 21st century, the initially colder surface waters enhance high latitude surface heat fluxes from the atmosphere into the ocean, resulting in a global ocean heat uptake anomaly of 60 ZJ by 2100. The AMOC shows an additional reduction of 1 Sv during the 21st century, mainly effecting the heat content of the Arctic basin.

Keywords ice sheet freshwater · AMOC · Ocean Heat Uptake

M.A.J. Stoffelen
Institute for Marine and Atmospheric Research Utrecht,
Dept. of Physics and Astronomy, Utrecht University,
Princetonplein 5, 3584 CC Utrecht, The Netherlands.
E-mail: m.a.j.stoffelen@uu.nl

1 Introduction

When the energy balance of Earth's climate system is perturbed by increased atmospheric greenhouse gas (GHG) concentrations, the system will distribute the excess heat over its various components and will adjust towards a new equilibrium. Currently, over 90% of Earth's energy surplus enters the surface ocean, part of which is transported away from the surface to the ocean interior. As the energy in the deep ocean is stored there on timescales ranging from centuries to millennia, the effectiveness of the vertical ocean heat transport determines the amount of heat that resides in the mixed layer and thereby sets the pace of transient global warming in the coming century.

Previous studies have found that on a global scale the ocean heat budget is dominated by downward advection of heat (i.e. downwelling waters are warmer than upwelling waters, on average) that is compensated by upward transport of heat by diffusion along sloping isopycnals and deep convection, both in the Southern Ocean and the North Atlantic (e.g. Gregory [2000], Gnanadesikan and Slater [2005], Hieronymus and Nycander [2013]). Ocean heat uptake (OHU) under increasing CO_2 scenarios is found to be dominated by reduced convection and isopycnal diffusion [Huang et al, 2003], both in response to an increase in stratification due to reduced surface heat loss and increased precipitation at high latitudes [Banks and Gregory, 2006]. It thus seems that high-latitude buoyancy fluxes play an important role in OHU and the rate of climate warming.

The Greenland and Antarctic ice sheets (hereafter GrIS and AIS, respectively) could therefore play a crucial role in transient climate simulations. They discharge freshwater along their margins in the form of icebergs,

surface runoff and basal meltwater coming of ice shelves, at locations close to regions of deep convection and formation sites of deep ocean water masses.

To directly assess the impact of ice sheet freshwater fluxes on OHU, a coupling of the surface mass balance and calving processes to a general circulation model is needed. However, none of the climate models that participated in the Coupled Model Intercomparison Project Phase 5 (CMIP5) has an interactive ice sheet or snow component. The potential consequences of increased ice sheet melt have therefore been assessed in model studies using prescribed freshwater fluxes, but these were highly idealized in terms of either spatial distribution, magnitude and temporal variability of the freshwater forcing. To isolate the impact of the additional freshwater, most of these studies were performed under fixed CO_2 forcing.

In this study, we incorporate a best estimate of ice sheet freshwater forcing into a state-of-the-art Earth System Model, for the past as well as two different climate scenarios of the future (in total, the period 1850-2200 is simulated). This freshwater forcing is based on the most recent observational reconstructions and regional climate modeling efforts, employs a detailed GrIS runoff parametrization [Lenaerts et al, 2015] for the future and has a realistic seasonal cycle. Details of the experimental design are explained in section 2.

In section 3.1 we analyze some features of control experiments that use the model's original freshwater representation, before comparing them in section 3.2 with the simulations with the improved freshwater forcing. We go into more detail on the connections between anomalies in AMOC, ocean heat distribution and global temperatures in section 3.3. In section 4 we look at the correlation between AMOC and meridional density difference. In section 5 an attempt is made to quantify the effect of the anomalous heat uptake on climate sensitivity. A summary and discussion is presented in section 6.

2 Experimental design and model description

2.1 Model description

The climate model used in this study is the Community Earth System Model (CESM, version 1.1.2.) with a nominal horizontal resolution of approximately 1 degree. The set up is similar to the CESM simulations used for CMIP5 [Meehl et al, 2013], but is updated to a more recent model version and uses the ozone forcing of Marsh et al [2013]. Its atmospheric component is the Community Atmosphere Model version 5 (CAM5) and has 30 vertical levels. The ocean component is the Parallel Ocean Program version 2 (POP2) and has 60 levels. The land module (Community Land Model version 4, CLM4) includes coupling of carbon and nitrogen processes between climate and terrestrial ecosystems. To improve energy conservation, CESM splits ice sheet and glacier mass loss into separate liquid water and solid ice fluxes that are passed to the ocean component. The sea ice component is the Los Alamos Sea Ice Model version 4 (CICE). Many aspects of fully coupled simulations performed with similar configurations of CESM are documented in a special collection of the *Journal of Climate* (see http://journals.ametsoc.org/page/CCSM4/CESM1).

2.2 Climate scenarios

In this study we analyze simulations by CESM of the period 1850-2200, driven by historical emissions (1850-2005) and two future (2006-2200) climate scenarios, the Representative Concentration Pathways 2.6 (RCP26) and 8.5 (RCP85) and their extensions after 2100 [Meinshausen et al, 2011]. These simulations are initialized after running a 1500 year control simulation under preindustrial forcing. Timeseries of atmospheric CO_2 concentrations in our simulations are shown in Figure 1a. RCP26 is characterized as a "peak-and-decline" scenario with a maximum CO_2 concentration of approximately 450ppmv by mid-21st century followed by a sustained decrease in the 22nd century. The RCP85 scenario is characterized by a strong and sustained increase in CO_2 over time, reaching 950 ppmv by 2100. After 2120, the original extension of the scenario is modified by fixing atmospheric CO_2 concentrations at ∼1100ppmv, about 4 times the preindustrial value. Note that all other greenhouse gases represented in the model's radiative transfer (CH_4, N_2O, CFC-11 and CFC-12) follow the original pathways of Meinshausen et al [2011].

2.3 Freshwater forcing

2.3.1 CTRL simulations

The original representation of ice sheet freshwater fluxes in CESM, as used in our CTRL simulations, is based on a mass conservation principle. In the absence of ice dynamics, the precipitation that falls on the ice sheet and that is not stored in the snow model, is instantaneously discharged as solid ice into the nearest ocean grid point, representing calving processes. Meltwater that is generated when surface temperatures are above zero, will also run off into the ocean if it does not refreeze in the snow layer. As the snow model has a maximum capacity of $1000\,\mathrm{kg\,m^{-2}}$, i.e. a thickness of roughly 3 m

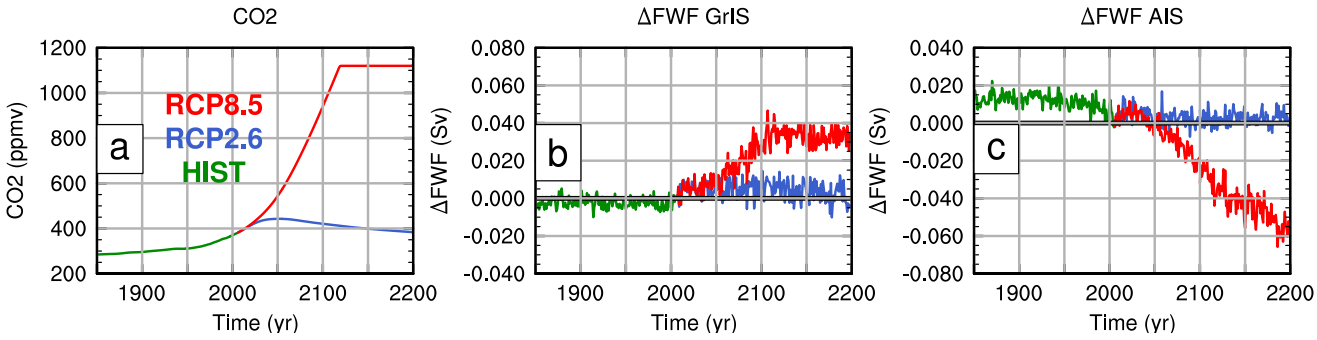

Fig. 1 Time series of annual average (a) CO_2 concentrations, ΔFWF, the difference in ice sheet freshwater flux between FWF and CTRL runs (FWF − CTRL) from (b) the Greenland Ice Sheet and (c) the Antarctic Ice Sheet, for the climate scenarios as labeled by color.

of snow, the ice sheets cannot grow over time and any enhancement of precipitation or melt over these areas will result in increased freshwater fluxes to the ocean. This is very relevant for the AIS, as CESM, like other general circulation models (GCMs), simulates an enhanced hydrological cycle at high latitudes. In CTRL, this leads to increased AIS freshwater fluxes, which ignores the large refreezing capacity of the AIS that lets most of the extra precipitation just accumulate on the continent [Ligtenberg et al, 2013].

2.3.2 FWF simulations

In our FWF simulations, we replace both the solid and liquid freshwater fluxes from the ice sheets to the ocean with best estimates based on observations, regional climate modeling and a GrIS runoff parametrization.

Our GrIS solid ice discharge distribution is constructed following Enderlin et al [2014], who used remote sensed observations to estimate discharge from 178 individual GrIS glaciers over the period 2000-2012. Each glacier discharge flux is assigned to the nearest ocean grid point. The short time period of observations and the strong stochastic variability in ice sheet dynamics prevent a clear assessment of long-term trends of ice discharge [Wouters et al, 2013], and therefore we keep the GrIS ice discharge constant in time.

The construction of GrIS surface runoff is based on output of the regional atmospheric climate model RACMO, version 2.1 (RACMO2). For the period 1960-2012, the model was forced at its lateral boundaries by atmospheric fields of the ERA-Interim reanalysis and a CMIP5 general circulation climate model (HadGEM2-ES), and we use its surface mass balance (SMB) calculations to construct annual average surface runoff. As data prior to 1960 is sparse, we assume that GrIS runoff in the period 1960-1989 was representative for the years 1850-1959, and that this time series obeys a normal distribution so as to impose realistic interannual variability.

Future GrIS surface runoff in the two climate scenarios is constructed from the parametrization described in Lenaerts et al [2015]. There, second order correlation coefficients were determined for the runoff in 8 different basins of the GrIS as a function of mid-tropospheric (500hPa) summer temperature anomalies (T500), making use of a simulation of RACMO2 under the mid-way RCP4.5 climate scenario. The significant correlations seem robust over a wide range of scenarios [Fettweis et al, 2013] and we use them here to calculate annual average surface runoff from the T500 time series of the CTRL runs.

On the annual average GrIS surface runoff time series of the whole 1850-2200 period, we impose a seasonal cycle at monthly resolution, with a runoff peak in summer and little to no runoff in winter. The imposed cycle is the average seasonal cycle of the 1960-2012 runoff from the RACMO2 simulation described above, that is scaled to annual averages of each year.

For the AIS, freshwater fluxes in our FWF simulations are based on Depoorter et al [2013], who estimated the mass balance components of all the ice shelves of Antarctica exceeding 100 km^2, using satellite measurements of calving and grounding line fluxes and RACMO2 model results for snow accumulation [Lenaerts et al, 2012]. They concluded that iceberg calving and subsurface melting by the ocean are both responsible for roughly 50% of the gross mass loss of the AIS, but with large regional differences. In this study, these components are added as a single solid ice flux into the ocean. There is evidence that enhanced outflow currently outweighs any increase in snow accumulation, but no reliable projections can be made for this 21st century due to uncertainty in ice dynamics [Church et al, 2013]. Therefore, we only incorporate the recently observed increase in outflow in the Amundsen basin and let it stabi-

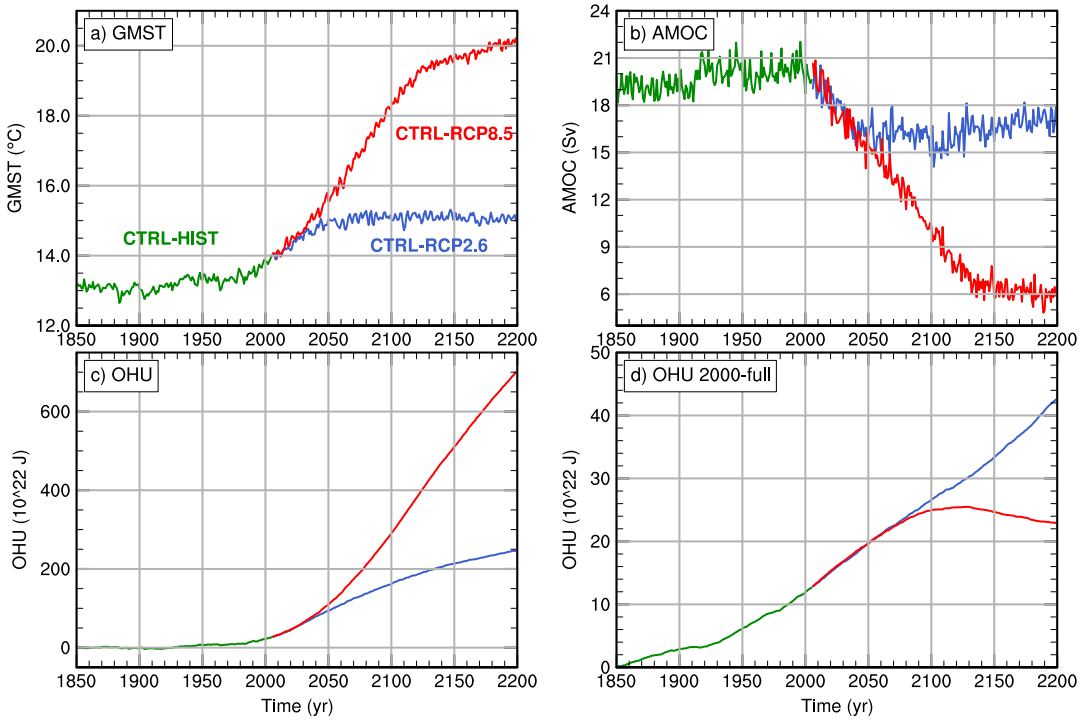

Fig. 2 *CTRL runs.* Time series of annual mean (a) globally averaged surface air temperature, (b) AMOC index (maximum Atlantic meridional overturning streamfunction at 26.5N and below 500m depth), (c) heat uptake for the global ocean and (d) the ocean below 2000m, both referenced to 1850. Climate scenarios labeled by colors in (a).

lize after 2020 at a higher calving rate, equivalent with a 0.005 Sv increase in freshwater flux (1Sv $=10^6\,\mathrm{m}^3\,\mathrm{s}^{-1}$). The rest of the calving rates is kept constant. Liquid water runoff is set equal to zero, as regional climate model studies show that almost all surface-generated meltwater refreezes in the snowpack before reaching the ocean [Ligtenberg et al, 2013].

2.3.3 Net difference

Figure 1b shows the net difference in freshwater forcing (FWF − CTRL) coming from the GrIS. The differences during the historical period are very small, showing that CESM provides realistic GrIS freshwater fluxes in present day conditions. In the warming scenarios ΔFWF is generally positive. For RCP26, calving rates are slightly higher in CTRL than in FWF, offsetting most of the increased surface runoff (separate contributions not shown). In RCP85, the increase in surface runoff is much stronger, resulting in a total freshwater forcing of almost 0.04 Sv around 2100. As the RCP85 GHG forcing levels off at 2120, so does the freshwater forcing.

The difference in freshwater forcing for the AIS during the historical period (Figure 1c) is about 0.015 Sv, mainly as a result of a higher calving flux in FWF (the surface runoff starts at almost zero in CTRL). As apart from the increased outflow in the Amundsen basin, the FWF freshwater forcing stays constant, the growing deficit in freshwater as shown for RCP85 is attributed to an increase in precipitation over the AIS that the model can not store on the continent.

Thus in the strong warming scenario, our best estimate freshwater fluxes from the GrIS are *larger* than CTRL, while the fluxes from the AIS are *smaller*. In absolute terms the contribution from the AIS dominates, resulting in a freshening of the World Ocean in RCP85.

3 Results

3.1 CTRL run

We begin with an analysis of the CTRL runs, to show the overall response of the model to the greenhouse gas forcing in the different climate scenarios. Figure 2 shows the global mean surface air temperature (GMST), Atlantic meridional overturning circulation index (AMOC) and the global and deep ocean heat uptake (OHU) for the CTRL runs.

GMST (Figure 2a) rises in response to GHG forcing during the 20th century, with an increasing rate until the scenarios start to diverge around 2030. Under

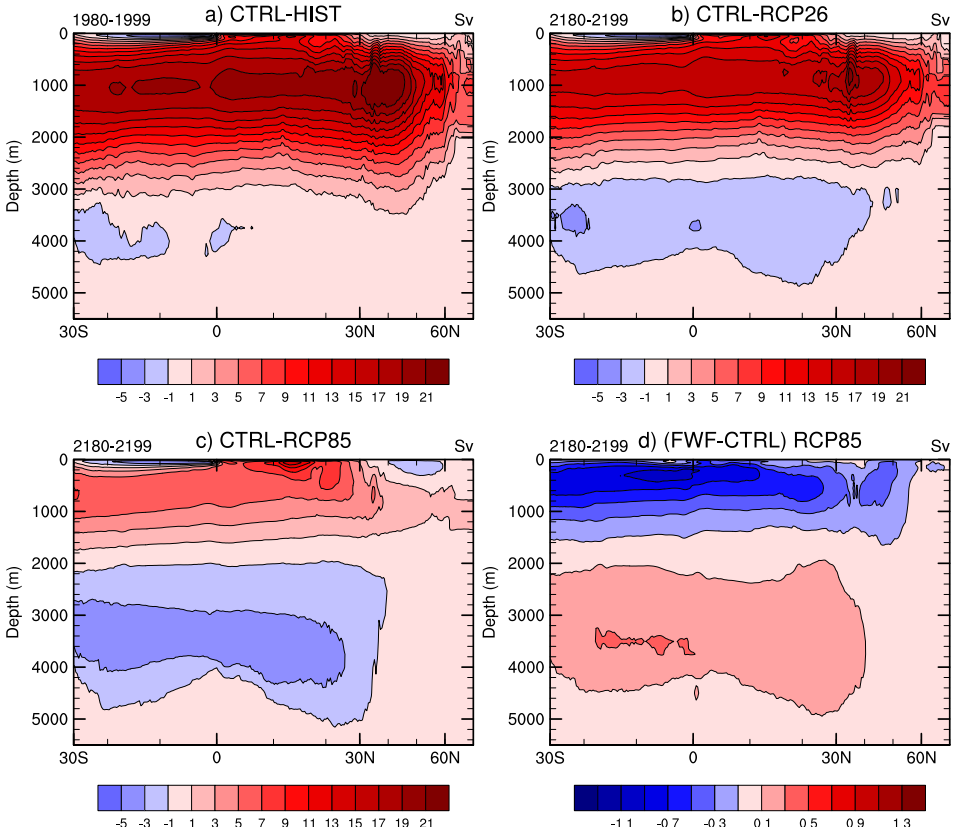

Fig. 3 Atlantic meridional overturning streamfunction averaged over 20 years (a) at the end of the 20th century, at the end of the 22nd century (b) under RCP26 and (c) under RCP85, with red (blue) colors indicating clockwise (anticlockwise) transport. Panel (d) shows the 20 year averaged difference in this streamfunction at the end of the 22nd century between FWF-RCP85 and CTRL-RCP85.

RCP26, the GMST levels off during the 21st century to just above 15 °C, a 2 °C increase with respect to 19th century values. Under RCP85, temperature keeps rising at a rate of about 0.5 °C/decade until we fix the CO_2 concentration in 2120, after which the rate of warming decreases to approximately 0.1 °C/decade.

The AMOC index, defined here as the maximum of the Atlantic meridional overturning streamfunction at 26.5N and below 500 meters depth, is displayed in Figure 2b. In the historical period, the AMOC strength of ∼20 Sv is somewhat higher than observed along the RAPID monitoring array (17.5 Sv for the period 2004-2012 [Smeed et al, 2014]). Both future scenarios show a significant decrease in overturning strength in the 21st century. In RCP26, AMOC reaches a minimum of 15 Sv around 2100, after which it partially recovers during the 22nd century. The overturning in RCP85 shows a strong linear decrease until 2130, after which it keeps weakening at a slower rate, reaching a minimum of 6 Sv at the end of the simulation.

Figures 2a and 2b show that there is a strong negative correlation between AMOC and global warming. This is in line with Jahn and Holland [2013], who showed that the AMOC strength in CCSM4, the predecessor of CESM, is inversely proportional to the applied CO_2 forcing. They showed that the weakening of the AMOC is caused by a reduction of North Atlantic deep convection due to a surface freshening. The freshening of the Labrador Sea in their study comes from influx of melted Arctic sea ice due to the warming. Note that in this view, global warming is the cause of freshening of the North Atlantic that in turn weakens the AMOC. This is different from the analysis in section 3.2, where we investigate the impact of additional freshwater coming off the GrIS that is added artificially.

Figure 2c shows the ocean heat uptake since 1850 for the global ocean. This OHU signal is similar to the surface air temperature, albeit it is a lot smoother, reflecting the long adjustment timescale of the ocean compared to the atmosphere. The amount of heat stored in the ocean reaches about 2500 ZJ in RCP26 and 7000 ZJ in RCP85 at the end of the simulations.

Remarkably, the warming of the deep ocean below 2000m (Figure 2d) is independent of climate scenario until 2070, and afterwards becomes substantially larger in RCP26 than in RCP85, contrary to the overall warm-

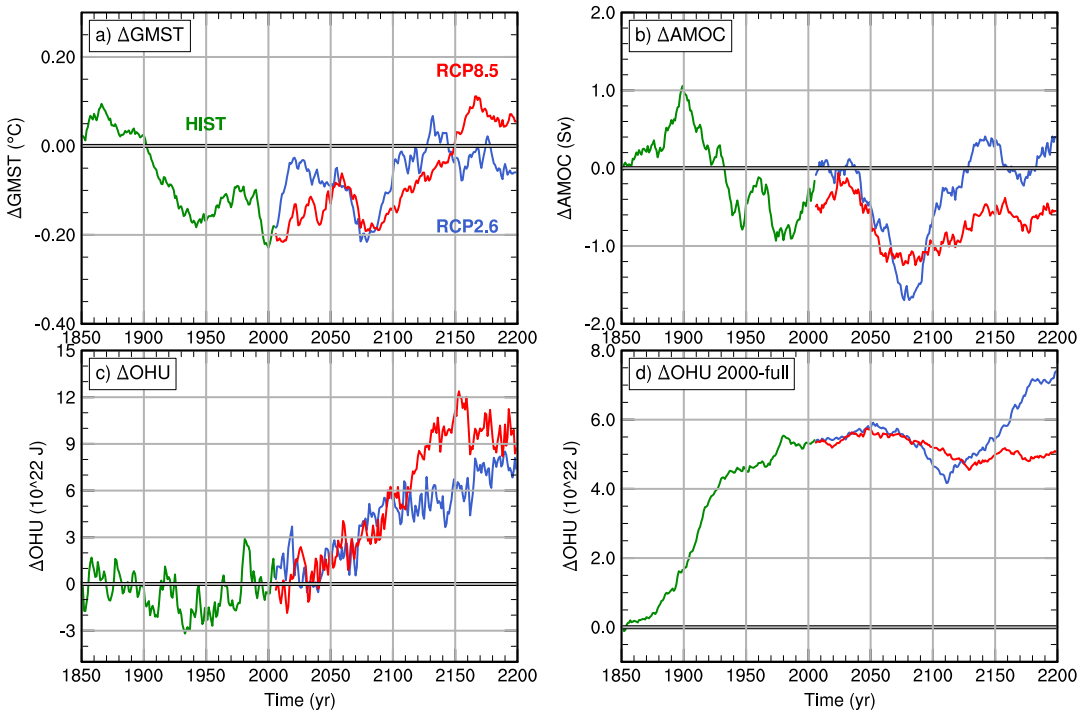

Fig. 4 *FWF-CTRL*. Panels show differences between FWF and CTRL simulations, for the same variables as in Figure 2: ΔGMST (a), ΔAMOC (b), ΔOHU full depth (c) and ΔOHU below 2000 meters (d). A 20 year running average is applied to ΔGMST and ΔAMOC, while annual averages are shown for ΔOHU (global and deep). The colors are labeled in panel (a).

ing trend for the full ocean. Despite the enormous heat entering the ocean in RCP85, the deep ocean slightly cools after 2130. The source of these differences lies in the Atlantic basin, and seems to be related to different weakening and shallowing of the AMOC, shown in Figure 3. In RCP26 (3b) the upper cell of the AMOC shallows only a few hundred meters compared to the end of the 20th century (3a), while in RCP85 (3c) it contracts completely to above 2000 m depth. Propagation of the global warming signal to the deep ocean by advection is therefore strongly inhibited in RCP85. Expansion and strengthening of the lower AMOC cell cools the tropical deep Atlantic basin by intrusion of relatively cold Antarctic Bottom Water (AABW).

3.2 FWF minus CTRL

We continue our analysis by looking at the differences between the FWF and CTRL runs, in order to investigate the impact of the freshwater scenario on transient climate change. All anomalous timeseries in this section are labeled with a Δ-symbol and indicate FWF *minus* CTRL. Figure 4 shows the differences in GMST, AMOC and global and deep OHU caused by differences in freshwater forcing.

Starting from zero, ΔGMST (Figure 4a) becomes slightly negative during the historical period and fluctuates around an anomaly of $-0.15\,^{\circ}$C between 1930 and 2100 for both RCP26 and RCP85, after which the anomaly goes back to zero at the end of the 22nd century. It is interesting to note that ΔGMST evolves in a similar fashion in both climate scenarios, although ΔFWF (Figure 1) differs substantially.

Timeseries of ΔAMOC are given in Figure 4b and show a generally weaker AMOC in the FWF runs, the difference in the overturning strength being on the order of 1 Sv. The pattern of AMOC weakening is similar to that of the AMOC itself (Figures 3c and 3d), indicating an overall reduction in strength and not a spatial shift. These relatively small effects indicate that AMOC weakening in the next century is dominated by direct effects of global warming on deep water formation, and that realistic amounts of GrIS melting would only slightly enhance this.

We first investigate if ΔAMOC and ΔGMST are correlated in a similar fashion as their absolute counterparts discussed earlier. On the annual average timeseries of both quantities, we first apply linear detrending (separate for the 3 simulations HIST, RCP26, RCP85), in order to reduce the nonstationary effects of the background AMOC. We then divide the timeseries into 11-

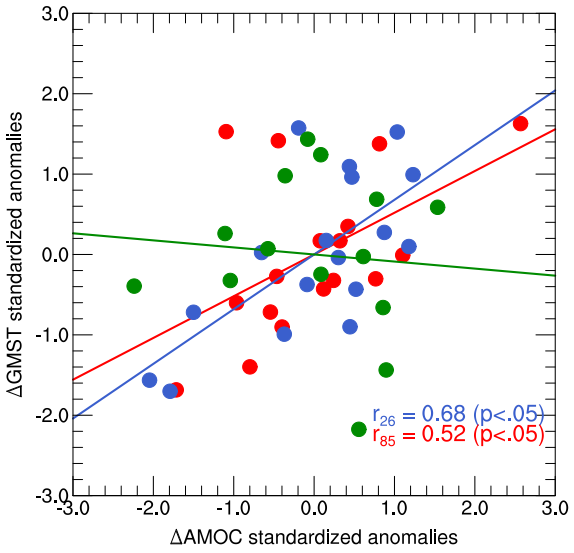

Fig. 5 Standardized anomalies of ΔGMST versus standardized anomalies of ΔAMOC, after linear detrending and averaging over fixed windows of 11 years. Historical data in green, RCP26 in blue and RCP85 in red. Significant (p<.05) sample correlation coefficients of 0.68 and 0.52 for RCP26 and RCP85, respectively.

year windows and average over each window. Finally, we calculate standardized anomalies for each quantity. The result of this is shown in Figure 5. We find significant ($p < 0.05$) correlations in RCP26 and RCP85 of 0.68 and 0.52, respectively, while no significant result is found in HIST. The correlations between ΔAMOC and ΔGMST are positive, meaning that a negative overturning anomaly is associated with a negative temperature anomaly, opposite to the negative correlations found in section 3.1.

Figure 4c and 4d show the difference in ocean heat uptake between our FWF and CTRL simulations for the global and the deep (2000m+) ocean, respectively. Over the whole historical period, there is little difference in net heat uptake, while the deep ocean becomes considerably warmer in FWF compared to CTRL. This indicates a vertical redistribution of heat. Note that both simulations are branched off from the same spin-up, so the deep ocean trend cannot be explained by a too short spin-up time.

After year 2000, ΔOHU is positive and increases with the same rate in both climate scenarios reaching 60 ZJ in 2100, after which the two signals diverge. This indicates that the best estimate freshwater scenario enhances the future uptake of heat by the ocean, compared to the CTRL simulations. In the deep ocean the difference in stored heat does not change much during the 21st century but increases by ~20 ZJ in RCP26 after 2100. Note that at the end of the simulations, between 55% (RCP85) and 94% (RCP26) of the anomalous global heat uptake is stored below 2000m.

3.3 Connecting circulation, heat storage and temperature

In the previous section we reported 2 important findings while comparing the FWF and CTRL simulations, namely (1) that there is a vertical redistribution of ocean heat during the historical period, storing more heat at depth in FWF and (2) that in the future, more heat is taken up by the global ocean in FWF. In this section we further analyze these results and explain possible mechanisms.

To clarify the internal, vertical redistribution of heat during the historical period, we calculate differences in surface, deep and total heat uptake for different basins (Figure 6) of the World Ocean. Marginal seas are excluded from our analysis. Results are shown in Figure 7.

We see that immediately from the start of the simulations, the deep Southern Ocean develops a positive heat anomaly that grows to a maximum of 20 ZJ in 2000. A similar positive heat anomaly develops at depth in the other basins, but at a delay of a few decades.

We argue that the deep ocean heat anomaly is due to a decrease in AABW formation as a result of the positive AIS freshwater anomalies during the historical period (Figure 1c). This reduces the cooling effect of Southern Ocean deep convection, effectively warming the bottom waters. This anomaly is then transported to the other basins by the bottom overturning cell.

An indication for reduced AABW formation during the historical period is the negative anomaly in mixed layer depth around the Antarctic continent, shown as the 1850-1900 average in Figure 8. This pattern in mixed layer depth is persistent during the historical period. Note that these are annual averages, with wintertime mixed layer depth anomalies likely being stronger but not calculated here.

The relative warming of the deep ocean is accompanied by a cooling of the overlying waters in all basins (Figure 7, left column), with the largest heat losses coming from the Pacific basin and a substantial contribution by the Indian Ocean. Globally, the surface waters reach a minimum around 2000 but stay anomalously cold during the whole 21st century (Figure 7, topleft). This cold surface water anomaly is tightly coupled to the surface air temperature anomaly (Figure 4a), which suggests that the decrease of ΔGMST during the historical period is a consequence of AIS freshwater anomalies and not related to AMOC to first order, in agreement with Figure 5.

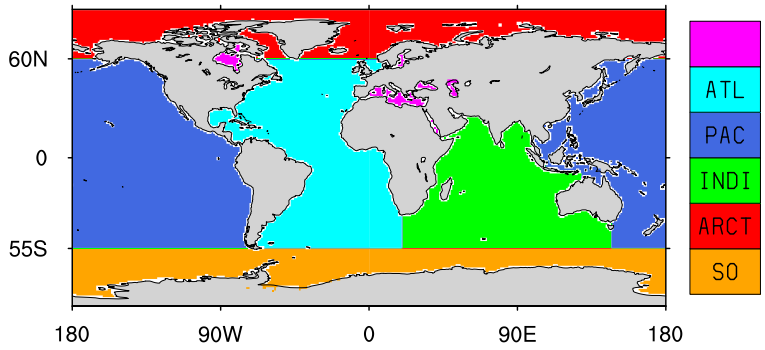

Fig. 6 Overview of the different ocean basins used for Figure 7: Atlantic (cyan), Pacific (blue), Indian (green), Arctic (red) and Southern Ocean (orange). Marginal seas (not included in heat content analysis) in magenta.

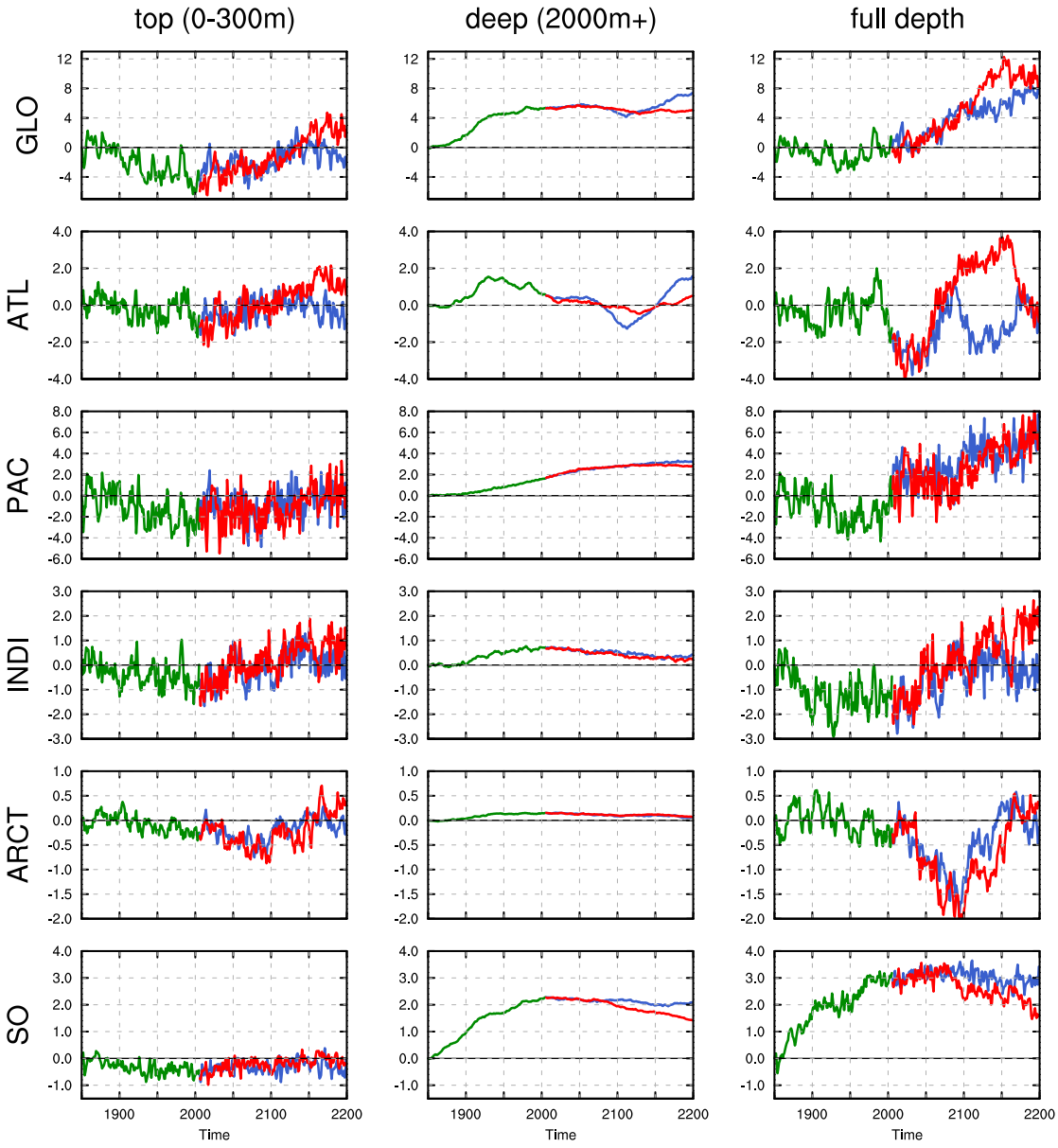

Fig. 7 ΔOHC, the difference in ocean heat content (FWF-CTRL) referenced to 1850, in units of 10^{22} J, for 3 different layers (from left to right: 0-300m, deeper than 2000m, full depth) and 6 different basins (from top to bottom: Global, Atlantic, Pacific, Indian, Arctic and Southern Ocean). Historical period in green, RCP26 in blue and RCP85 in red.

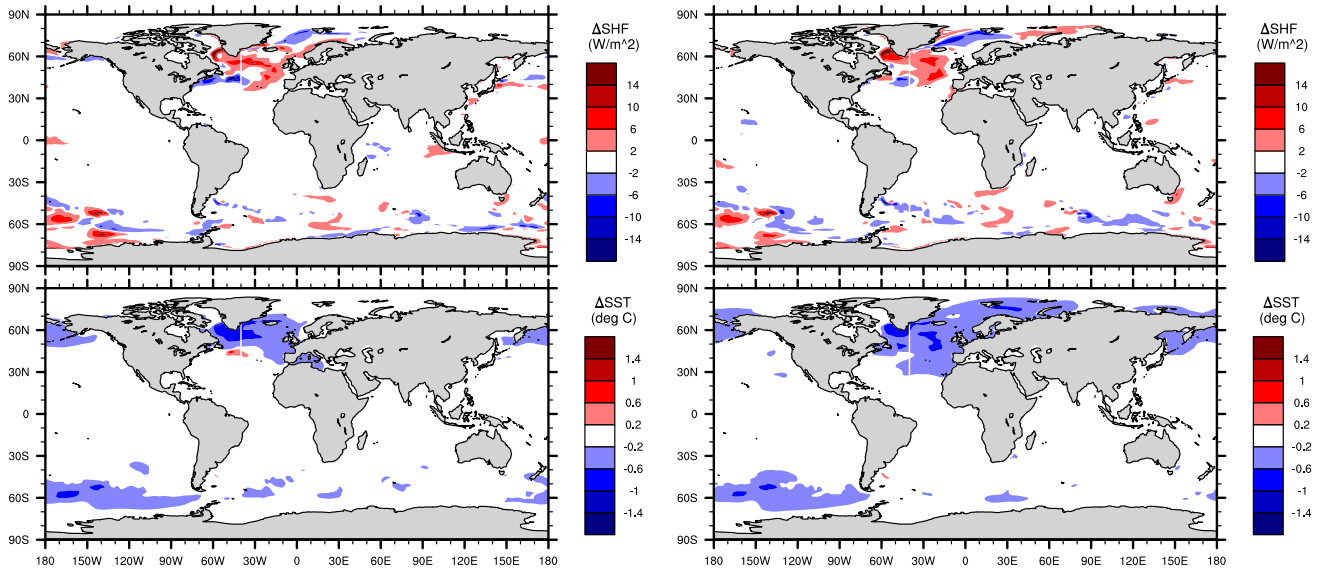

Fig. 9 Top row: ΔSHF, the difference in surface heat flux between FWF and CTRL, with positive values indicating heat entering the ocean. Bottom row: ΔSST, the difference in sea surface temperature between FWF and CTRL. Results for RCP26 on the left and RCP85 on the right. All variables averaged over years 2006-2099.

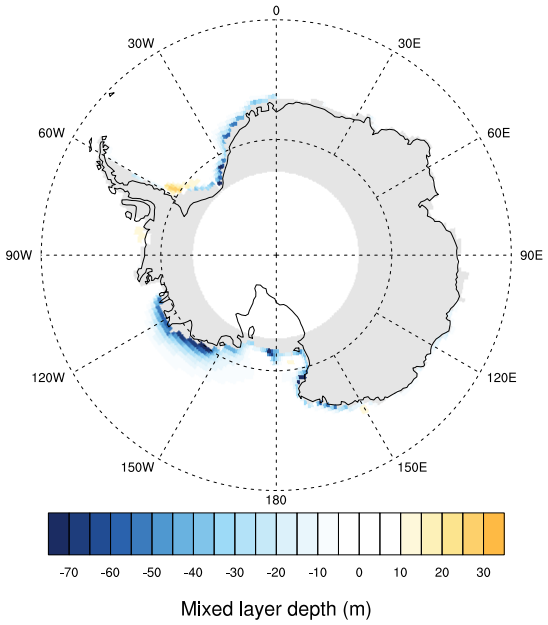

Fig. 8 Difference in the annual average mixed layer depth in the Southern Ocean between FWF and CTRL, averaged over 1850-1899.

The colder surface waters are likely to affect Earth's radiation balance by reduced outgoing longwave radiation (OLR) and possibly an increase of albedo due to a larger sea ice extent. These effects should be analyzed further before a complete picture of the energy fluxes can be given.

To see where the future difference in heat content between the FWF and CTRL simulations (Figure 4c) comes from geographically, we map the 21st century average of the total surface heat flux anomaly (ΔSHF) under both climate scenarios in Figure 9 (top row). Positive values (red) indicate heat going into the ocean. We see that the two main locations where anomalous heat enters the ocean are the Atlantic north of 40°N and the Southern Ocean between 130°W and 180°W. As expected from the net increase in global ΔOHU during this period, the heat fluxes in these areas are not fully compensated elsewhere.

The regions of positive ΔSHF coincide with regions with a negative sea surface temperature anomaly (ΔSST), as shown in Figure 9 (bottom row). This is to be expected, as cooler SSTs result in reduced OLR, a larger sensible heat flux from the atmosphere into the ocean and a reduced outgoing latent heat flux as there is less evaporation. Although in agreement with the cold GMST anomaly of Figure 4a and the upper ocean heat anomalies of Figure 7, it is remarkable that ΔSST is nowhere strongly positive.

To summarize some of the previous results, we propose the following storyline explaining the relation between ΔGMST and ΔOHC between 1850 and 2100. During the historical period, deep sinking around Antarctica is reduced due to the extra freshwater coming off the AIS, effectively warming the deep Southern Ocean from the start of the simulations and the other basins on an advective timescale. The surface waters as well as the GMST become anomalously cold, showing a negative trend over the whole historical period. If this is only an internal redistribution of heat remains an open question, as the effects on e.g. sea ice extent are not studied

here. When the climate starts to warm at the end of the 20th century, the colder upper ocean can take up heat more efficiently in FWF, as shown by the increased surface heat fluxes over regions with colder SSTs. This is accompanied by a recovery to zero of both upper ocean temperature anomalies as well as ΔGMST. The anomalous global ocean heat uptake of 60 ZJ by 2100 resides for the most part in the deep ocean.

4 AMOC - meridional density gradient

Many modeling and theoretical scaling studies suggest that changes in the AMOC can be understood in terms of a simple causative relation between AMOC and the meridional density gradient [Rahmstorf [1996], Thorpe et al [2001]]. The rational behind this comes from scaling of the thermal wind relation which leads, under some assumptions carefully reviewed by Boer et al [2010], to

$$\mathrm{AMOC} = \frac{gH^2}{\rho_0 f_0}\Delta\rho, \tag{1}$$

where $\Delta\rho$ is the meridional density difference across the basin, H is the scale depth, ρ_0 is a reference density and f_0 is a typical value for the Coriolis parameter.

Different closure schemes for the scale depth, often assumed to be equal to the thermocline depth, have been suggested. The simplest approach, assuming H to be constant, leads to a linear relation between AMOC and $\Delta\rho$. The thermocline depth does not have to be constant however, and if it is dependent on $\Delta\rho$ as a result of the flow, a nonlinear relation between overturning and meridional density difference emerges. It is not within the scope of this work to give a thorough exposition of all the different scaling relations existing in the literature, instead the reader is referred to Boer et al [2010] and Butler et al [2015] for recent overviews.

Figure 10 shows the correlation between our AMOC index and $\Delta\rho$, here defined as the potential density difference at 1000 meters depth between a Northern (50-55N) and Southern (35-40S) Atlantic box. It shows a quasi-linear relationship over the full range of density change, but with significant departures, especially for RCP26 and for AMOC strengths between 9 and 14 Sv in RCP85, corresponding to the 2nd half of the 21st century (Fig. 2).

At this stage we are unable to attribute the departures from linearity to any specific process. Boer et al [2010] argues that the positive correlation might break down when a remote influence effects the depth of the overturning but not the meridional density gradient, and mentions changes in Southern Ocean wind stress or AABW formation rate as examples. Butler et al [2015] show that strong correlations between AMOC and $\Delta\rho$ are robust in steady state or under low frequency variations, but don't hold for high frequency, high amplitude transitions. The fast and strong decrease of AMOC as here in RCP85 might be such a transition that introduces a time lag between the two quantities.

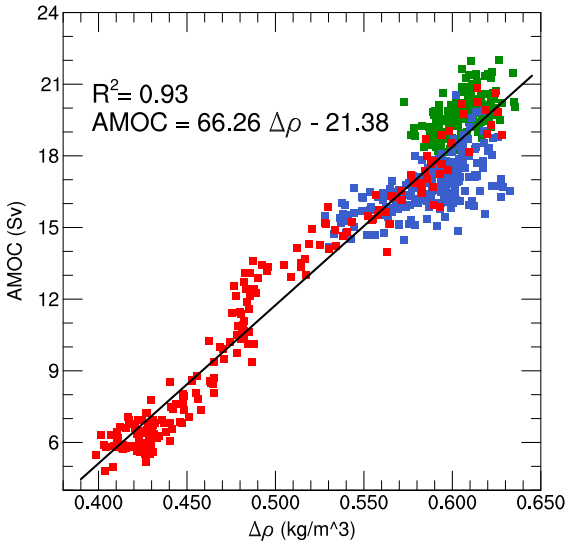

Fig. 10 Scatterplot of annual average AMOC index versus $\Delta\rho$, the annual average potential density difference at 1000 meters depth between a Northern Atlantic box (50-55N) and a Southern Atlantic box (35-40S). CTRL data only.

5 Climate Sensitivity

Equilibrium climate sensitivity (ΔT_{2x}) is defined as the equilibrium global mean surface air temperature change in response to the radiative forcing caused by a doubling of the CO_2 concentration (F_{2x}). ΔT_{2x} can be estimated directly from a climate model experiment where an inital steady state is perturbed by doubling the CO_2 concentration and the model is run until a new steady state is reached. This is not practical in state-of-the-art coupled models, as it takes thousands of years for the oceans to adjust.

Instead, we try to estimate climate sensitivity by the method proposed in Gregory et al [2004]. In general, the response of the climate system to a radiative forcing F can be assessed with a heat balance

$$N = F - \alpha\Delta T \tag{2}$$

where N is the net heat flux at the top of the atmosphere (Wm^{-2}, positive downward), ΔT is the global mean surface air temperature change (K) and α is the climate feedback parameter ($\mathrm{Wm}^{-2}\mathrm{K}^{-1}$), assumed to be constant over a large range of climate states and

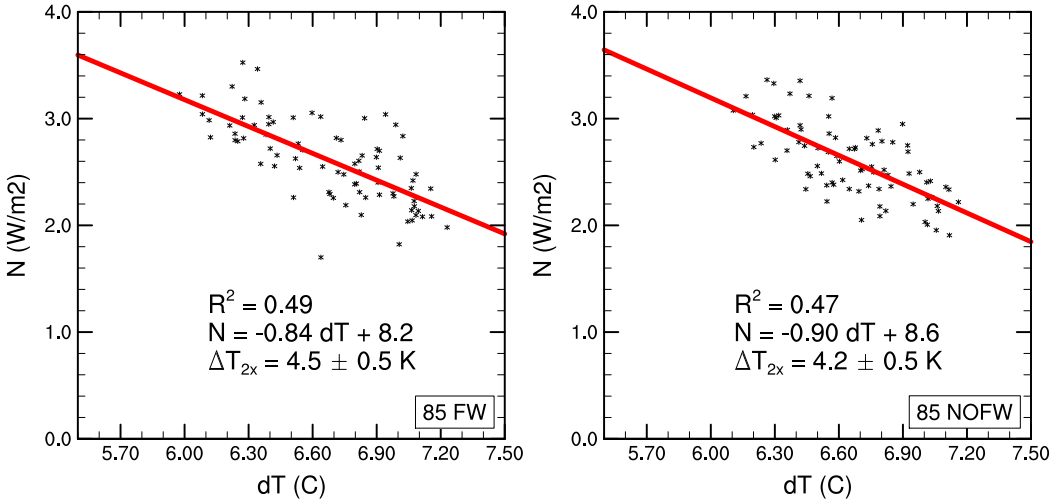

Fig. 11 Annual average top-of-atmosphere radiative imbalance N versus GMST change since 1850 in the RCP85 experiments for both FWF (left) and CTRL (right), for the years 2120-2199 for which CO_2 was held constant. The red line is a least square linear regression to this data.

forcings. From the models' output, N and ΔT can be directly calculated, but it is not straightforward to obtain F. If the forcing agent is constant in time (say, a fixed CO_2 concentration), the radiative forcing F can be assumed to be constant and a plot of N versus ΔT should result in a straight line, with a N-intercept of F and a slope equal to $-\alpha$.

In RCP26 the radiative forcing F is continuously varying and this method is not applicable. However, in the RCP85 experiment, the CO_2 concentration is held constant after 2120, and therefore provides a case to estimate climate sensitivity.

Figure 11 shows a scatterplot of the top-of-atmosphere radiative imbalance versus the global mean temperature change for the years where CO_2 is held constant. Linear regressions give the climate feedback parameters and combined with a standard "doubling" radiative forcing F_{2x} of $(3.74 \pm 0.04)\,\mathrm{W\,m^{-2}}$, we estimate equilibrium climate sensitivities of $\Delta T_{2\mathrm{x,FWF}} = (4.5 \pm 0.5)\,\mathrm{K}$ and $\Delta T_{2\mathrm{x,CTRL}} = (4.2 \pm 0.5)\,\mathrm{K}$.

These values are consistent with the equilibrium climate sensitivity of 4.10 °C reported by Meehl et al [2013] for the CESM configuration used for CMIP5. Because of the large uncertainty in the slope of the regression, we cannot detect a significant difference between the sensitivities found for FWF and CTRL.

6 Summary and Discussion

Using past and future simulations of the state-of-the-art Community Earth System Model, we studied the effects of a best estimate of ice sheet freshwater forcing, that was based on the most recent observational reconstructions and modeling efforts. Apart from the recently observed increased outflow of the Amundsen basin, we did not include future changes in iceberg calving for either ice sheet.

We showed that compared to control experiments, the positive AIS freshwater anomaly during the historical period reduces deep convection in the Southern Ocean, effectively warming the deep ocean, while the surface waters become anomalously cold. The question if this is just an internal redistribution, or that also the radiative balance is affected (e.g. by changes in the outgoing longwave radiation or sea ice extent) could not be answered and needs additional study.

Our results suggest that the perturbation around Antarctica influences the deep ocean on a global scale, although with a delay of a few decades. This lag is about as large as the total length of the experiments in Stammer [2008], who concluded from an ocean-only freshwater experiment that the global ocean is less sensitive to perturbations in surface buoyancy fluxes imposed to the Southern Ocean compared to the North Atlantic. Here the AIS freshwater anomaly of ∼0.01 Sv is present for 150 years in the absence of other large perturbations, which makes its effects visible in the heat content of all basins.

Due to the buildup of anomalously cool surface waters around year 2000, the anomalous surface heat flux into the ocean is positive during the 21st century. Because the heat content of the deeper ocean does not change a lot, there is a net heat uptake of the global ocean of ∼60 ZJ. While not the subject of this study, this uptake of heat would also be very relevant for global sea level rise.

The AMOC showed a slight additional reduction during the FWF experiments, but the overall impact of the freshwater anomaly on AMOC stability is small. The anomalous freshwater forcing from the GrIS had a maximum of 0.035 Sv under RCP85, comparable with the weakest freshwater perturbations in the hosing experiments of Hu et al [2009] using CCSM3 and the SRES A1B climate scenario. We can confirm their conclusion that under such small freshwater perturbations, the ocean surface warming caused by the increase in greenhouse gas concentrations is dominant for the evolution of the AMOC.

Acknowledgements This paper was written as a MSc research project by the first author. He likes to thank his supervisors Dewi Le Bars and Henk Dijkstra for the guidance and fruitful discussions during the project, Jan Lenaerts for commenting on the manuscript and Leo van Kampenhout for performing the simulations.

References

Banks HT, Gregory JM (2006) Mechanisms of ocean heat uptake in a coupled climate model and the implications for tracer based predictions of ocean heat uptake. Geophysical Research Letters 33(7):3–6, DOI 10.1029/2005GL025352

Boer D, Agatha M, Gnanadesikan A, Edwards NR, Watson AJ (2010) Meridional density gradients do not control the Atlantic overturning circulation. Journal of Physical Oceanography 40:368–380, DOI 10.1175/2009JPO4200.1, URL http://oro.open.ac.uk/25664/

Butler ED, Oliver KIC, Hirschi JJM, Mecking JV (2015) Reconstructing global overturning from meridional density gradients. Climate Dynamics DOI 10.1007/s00382-015-2719-6, URL http://link.springer.com/10.1007/s00382-015-2719-6

Church J, Clark P, Cazenave a, Gregory J, Jevrejeva S, Levermann a, Merrifield M, Milne G, Nerem R, Nunn P, aJ Payne, Pfeffer W, Stammer D, aS Unnikrishnan (2013) Sea level change. Climate Change 2013: The Physical Science Basis Contribution of Working Group I to the Fifth Assessment Report of the Intergovernmental Panel on Climate Change pp 1137–1216

Depoorter Ma, Bamber JL, Griggs Ja, Lenaerts JTM, Ligtenberg SRM, van den Broeke MR, Moholdt G (2013) Calving fluxes and basal melt rates of Antarctic ice shelves. Nature 502(7469):89–92, DOI 10.1038/nature12567, URL http://www.ncbi.nlm.nih.gov/pubmed/24037377

Enderlin EM, Howat IM, Jeong S, Noh MJ, Van Angelen JH, van den Broeke MR (2014) An improved mass budget for the Greenland ice sheet. Geophysical Research Letters 41(3):866–872, DOI 10.1002/2013GL059010

Fettweis X, Hanna E, Lang C, Belleflamme a, Erpicum M, Gallée H (2013) Brief communication Important role of the mid-tropospheric atmospheric circulation in the recent surface melt increase over the Greenland ice sheet. Cryosphere 7(1):241–248, DOI 10.5194/tc-7-241-2013

Gnanadesikan A, Slater R (2005) The energetics of ocean heat transport. Journal of Climate 18(2002):2604–2616, DOI 10.1175/JCLI3436.1

Gregory JM (2000) Vertical heat transports in the ocean and their effect on time-dependent climate change. Climate Dynamics 16:501–515, DOI 10.1007/s003820000059, URL http://centaur.reading.ac.uk/19441/

Gregory JM, Ingram WJ, Palmer Ma, Jones GS, Stott Pa, Thorpe RB, Lowe Ja, Johns TC, Williams KD (2004) A new method for diagnosing radiative forcing and climate sensitivity. Geophysical Research Letters 31(October 2003):2–5, DOI 10.1029/2003GL018747, URL http://centaur.reading.ac.uk/5543/

Hieronymus M, Nycander J (2013) The budgets of heat and salinity in NEMO. Ocean Modelling 67:28–38, DOI 10.1016/j.ocemod.2013.03.006, URL http://dx.doi.org/10.1016/j.ocemod.2013.03.006

Hu A, Meehl Ga, Han W, Yin J (2009) Transient response of the MOC and climate to potential melting of the Greenland Ice Sheet in the 21st century. Geophysical Research Letters 36(10):L10,707, DOI 10.1029/2009GL037998, URL http://doi.wiley.com/10.1029/2009GL037998

Huang B, Stone PH, Sokolov AP, Kamenkovich IV (2003) The deep-ocean heat uptake in transient climate change. Journal of Climate 16(9):1352–1363, DOI 10.1175/1520-0442-16.9.1352

Jahn A, Holland MM (2013) Implications of Arctic sea ice changes for North Atlantic deep convection and the meridional overturning circulation in CCSM4-CMIP5 simulations. Geophysical Research Letters 40(6):1206–1211, DOI 10.1002/grl.50183

Lenaerts JTM, Van Den Broeke MR, Van De Berg WJ, Van Meijgaard E, Kuipers Munneke P (2012) A new, high-resolution surface mass balance map of Antarctica (1979-2010) based on regional atmospheric climate modeling. Geophysical Research Letters 39(4):1–5, DOI 10.1029/2011GL050713

Lenaerts JTM, Bars DL, Kampenhout LV, Vizcaino M, Enderlin EM, Broeke MRVD (2015) Representing Greenland ice sheet freshwater fluxes in climate mod-

els. Geophysical Research Letters (May):1–9, DOI 10.1002/2015GL064738.Abstract

Ligtenberg SRM, van de Berg WJ, van den Broeke MR, Rae JGL, van Meijgaard E (2013) Future surface mass balance of the Antarctic ice sheet and its influence on sea level change, simulated by a regional atmospheric climate model. Climate Dynamics 41(3-4):867–884, DOI 10.1007/s00382-013-1749-1

Marsh DR, Mills MJ, Kinnison DE, Lamarque JF, Calvo N, Polvani LM (2013) Climate change from 1850 to 2005 simulated in CESM1(WACCM). Journal of Climate 26(19):7372–7391, DOI 10.1175/JCLI-D-12-00558.1

Meehl Ga, Hu A, Arblaster JM, Fasullo J, Trenberth KE (2013) Externally forced and internally generated decadal climate variability associated with the interdecadal pacific oscillation. Journal of Climate 26(18):7298–7310, DOI 10.1175/JCLI-D-12-00548.1, URL http://journals.ametsoc.org/doi/abs/10.1175/JCLI-D-12-00548.1

Meinshausen M, Smith SJ, Calvin K, Daniel JS, Kainuma MLT, Lamarque J, Matsumoto K, Montzka Sa, Raper SCB, Riahi K, Thomson a, Velders GJM, van Vuuren DPP (2011) The RCP greenhouse gas concentrations and their extensions from 1765 to 2300. Climatic Change 109(1):213–241, DOI 10.1007/s10584-011-0156-z

Rahmstorf S (1996) On the freshwater forcing and transport of the Atlantic thermohaline circulation. Climate Dynamics pp 799–811

Smeed Da, McCarthy GD, Cunningham Sa, Frajka-Williams E, Rayner D, Johns WE, Meinen CS, Baringer MO, Moat BI, Duchez a, Bryden HL (2014) Observed decline of the Atlantic meridional overturning circulation 2004-2012. Ocean Science 10(1):29–38, DOI 10.5194/os-10-29-2014

Stammer D (2008) Response of the global ocean to Greenland and Antarctic ice melting. Journal of Geophysical Research 113(C6):C06,022, DOI 10.1029/2006JC004079, URL http://doi.wiley.com/10.1029/2006JC004079

Thorpe RB, Gregory JM, Johns TC, Wood Ra, Mitchell JFB (2001) Mechanisms determining the {A}tlantic thermohaline circulation response to greenhouse gas forcing in a non-adjusted coupled climate model. Journal of Climate 14:3102–3116, DOI 10.1175/1520-0442(2001)014¡3102:MDTATC¿2.0.CO;2

Wouters B, Bamber JL, van den Broeke MR, Lenaerts JTM, Sasgen I (2013) Limits in detecting acceleration of ice sheet mass loss due to climate variability. Nature Geoscience 6(8):613–616, DOI 10.1038/ngeo1874, URL http://www.nature.com/doifinder/10.1038/ngeo1874